ARTICLE   OPEN

Threatening levels of cumulative stress due to hydroclimatic extremes in the 21st century

Filippo Giorgi[1], Erika Coppola[1] and Francesca Raffaele[1]

Hydroclimatic extremes, such as very intense precipitation and drought, are expected to increase with global warming, with their cumulative effects potentially posing severe threats for human and natural systems. We introduce a new metric of potential cumulative stress due to hydroclimatic extremes, the Cumulative Hydroclimatic Stress index (CHS), expressed in "equivalent reference stress years (ERSY)" (i.e., the mean annual stress during a present day reference period). The CHS is calculated for wet and dry extremes in an ensemble of 21st century Global Climate Model projections under the RCP8.5 and RCP2.6 greenhouse gas scenarios. Under the high-end RCP8.5 scenario, by 2100, increases in wet and dry extremes add ~155 ERSY averaged over global land areas (~125 for wet and ~30 for dry extremes), with wet hotspots (>250 added ERSY) throughout regions of Asia, Eastern Africa and the Americas, and dry hotspots (>100 added ERSY) throughout Central and South America, Europe, West Africa, and coastal Australia. Inclusion of population exposure in the stress index definition generates a maximum total (dry + wet) potential stress level exceeding 400 added ERSY over Africa, North America, and Australia, which are thus projected to be extremely vulnerable to increases in hydroclimatic extremes. Under the RCP2.6 scenario, which is close to the 2 °C global warming stabilization target set in the Paris agreement, the total hydroclimatic stress is considerably reduced.

npj Climate and Atmospheric Science (2018)1:18 ; doi:10.1038/s41612-018-0028-6

INTRODUCTION

Hydroclimatic extremes can have severe impacts on different socio-economic sectors, such as agriculture, water resources, health, ecosystem services, urban infrastructure, etc.[1,2] This issue is especially important within the global change context because different generations of twenty-first century global and regional climate model projections have consistently indicated a predominant increase of precipitation intensity and wet extremes, along with a decrease in the frequency of precipitation events, and thus a lengthening of dry periods.[3–11]

While the occurrence of individual extremes can have devastating impacts at a given time, the cumulative effect of events over time may be a dominant factor in determining the overall stress for a natural or socio-economic system, thereby challenging its resilience.[1,2] For example, there might be thresholds of cumulative stress leading to the collapse of the system or to impacts that are beyond sustainable adaptation options. Also, the cumulative stress is an integrator over time and, since it accounts for the temporal trajectory of changes in extremes, it can be an optimal measure of related risks.

Here we introduce a new metric of the cumulative potential stress due to hydroclimatic extremes, the Cumulative Hydroclimatic Stress index (CHS), which is described in the Methods section. We calculate the CHS for two types of events that can be expected to produce damage to economic activities and infrastructure:[1,2] extreme daily precipitation (the 99.9 percentile of the daily precipitation intensity distribution, or R99.9) and severe precipitation deficits (defined as a sequence of at least three consecutive months with negative precipitation anomalies, or precipitation deficits, greater than 25%, or D25). The CHS is expressed in units of "Equivalent Reference Stress Year (ERSY)", where the ERSY is a measure of the average annual potential stress due to extreme wet or dry events for a reference period representing present day conditions (see Methods). If for a certain period in the future the cumulative number of ERSY is larger than the value that would be obtained by cumulating the ERSY found for the reference period, then the excess number of ERSY is a measure of the additional potential stress induced by climate change.

We emphasize that here the CHS is calculated from a physical quantity, namely precipitation, assuming that the stress itself is proportional to the amount of extreme or deficit precipitation. As such, it is a measure of potential stress, or risk, and not of actual damage associated with the events, because clearly not all events described by the R99 and D25 metrics will necessarily result in damaging flood or drought. The index could however be generalized to become an Integrated Cumulative Hydroclimatic Stress index (ICHS) by including socio-economic information, for example population exposed to, and/or cost and damage associated with, the event. As an illustration of this point, here we calculate the ICHS by including population information as a measure of exposure (see Methods), which again results in a metric of potential stress rather than actual impact.

The values of the CHS and ICHS are calculated for an ensemble of 9 Global Climate Model (GCM) projections from the Coupled Model Intercomparison Project, Phase 5 (CMIP5,[12] supplementary Table S1), covering the period 1981–2100, where 1981–2010 is our reference period. Two greenhouse gas (GHG) concentration pathways are considered, the high-end RCP8.5 and the low end RCP2.6, which cover the overall CMIP5 range.[13] Population data are from the set of IIASA Shared Socioeconomic Pathways (SSPs,[14])

[1]Earth System Physics Section, The Abdus Salam International Centre for Theoretical Physics, 34151 Trieste, Italy
Correspondence: Filippo Giorgi (giorgi@ictp.it)

npj nature partner journals

npj

Threatening levels of cumulative stress due to hydroclimatic
F Giorgi et al.

2

where we use the SSP1 and SSP5 for the RCP2.6 and RCP8.5, respectively.[14] The GCM and population data are interpolated onto a common grid, here taken as the grid of the HadGEM2-ES model[15] (1.875° longitude × 1.25° latitude), which also defines the continental coastlines. Observations from the Unified Gauge-Based Analysis of Global Daily Precipitation (UGDP) gridded dataset[16] are used for model validation after interpolation on the same grid. The Methods section provides more details on the procedures used.

In the next section, we first provide a brief validation of our GCM ensemble in the simulation of the extremes considered in this work. We then calculate values of the CHS and ICHS for each year throughout the 21st century projections, both globally and over the different regions of Supplementary Figure S1, to investigate whether climate change due to increases in GHG concentration may enhance the stress associated with hydroclimatic extremes. The results are intercompared across the RCP2.6 and RCP8.5 scenarios to assess the gain achieved by reaching the 2 °C global warming stabilization target (compared to pre-industrial temperatures) set in the Paris agreement, which is in fact close to the RCP2.6 scenario. A discussion of the results and final considerations are then presented in the concluding section.

RESULTS

Our ensemble of CMIP5 GCMs was selected because of the availability of daily precipitation data for both the RCP8.5 and RCP2.6 scenarios, but it has already been shown to produce an ensemble-mean precipitation change signal in line with the full CMIP5 ensemble.[12] Here we assess the performance of the model ensemble in simulating the R99.9 and D25 metrics by comparing simulated and observed cumulative values for the reference period 1981–2010 (Fig. 1). It can be seen that the ensemble shows a generally good agreement with observations in the simulation of the spatial patterns of both cumulative R99.9 and D25. The main model deficiency is a tendency to underestimate the observed magnitudes of these two metrics over some areas with large cumulative values, such as sub-continental Africa for D25, or central North America and Central-Northern Asia for R99.9. This tendency for understimation of extremes appears consistent with previous analyses of GCMs, being related to the relatively coarse resolution of the models as well as inadequacies of the model representation of precipitation processes.[17–20] Despite this problem, however, the simulated values of cumulative R99.9 and D25 are in line with observations over the majority of land areas. We thus assess that the ensemble selected is suitable for the study of changes in cumulative extremes in 21st century climate projections.

In addition, even though, as we stressed above, our metrics are only based on precipitation amounts and are not intended to be measures of impact or actual damage, we tested their representativeness of available flood and drought records over Europe. Supplementary Figures S2a,b compare the number of events above the R99.9 threshold (threshold calculated from the full
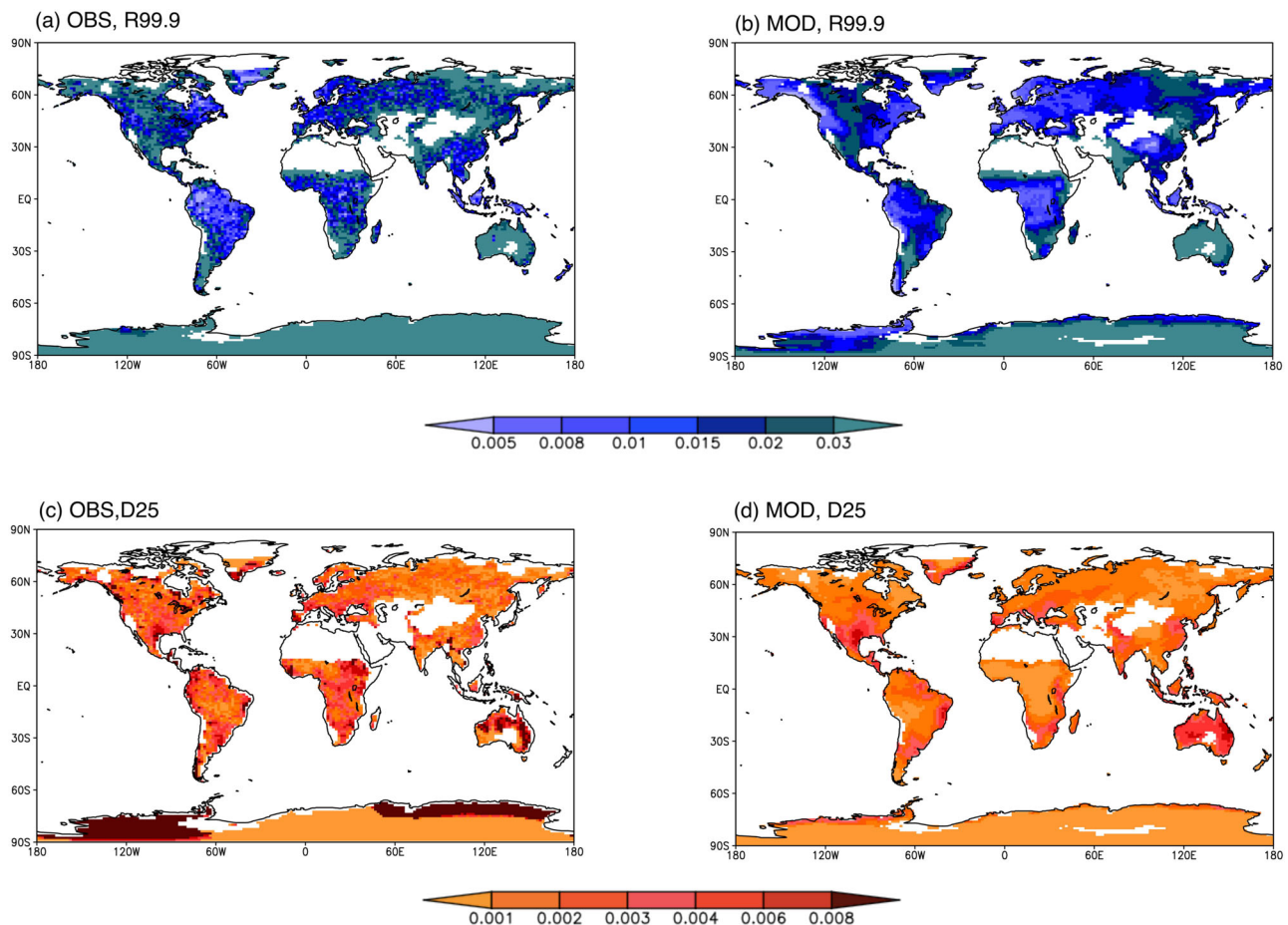

Fig. 1 a Observed cumulative R99.9. b Ensemble average simulated cumulative R99.9. c Observed cumulative D25. d Ensemble average simulated cumulative D25. Data are cumulated over the period 1980–2010 and units are fraction of total precipitation above the R99.9 or within the D25 anomalies

Threatening levels of cumulative stress due to hydroclimatic
F Giorgi et al.

npj

3

reference period 1986–2005) in our UGDP observational dataset with reported numbers of river floods by the European Environmental Agency (EEA) for the period 1998–2008 (http://www.eea.europa.eu/legal/copyright). In the observed flood report, 5 flood events or more occurred over southeastern Europe, southern England and areas of southern Germany, southeastern France, northeastern Italy and southern Georgia. By and large, taking into account the uncertainty in spatial placement due to the resolution of the data, the metric captures these areas of high flood numbers. We can also see however, that over some other areas, e.g., Scandinavia, the UGDP observations place the occurrence of R99.9 events that do not correspond to reported river floods. Figure S2c, d show a similar comparison between reported drought events over Europe in the period 2000–2009 and the corresponding value of the D25 metric for the years when the droughts were reported. Although in this case the comparison is necessarily qualitative due to the nature of the drought report information, we can still see that the metric generally captures the reported droughts. Supplementary Figure S2 thus illustrates how the R99.9 and D25 metrics are generally representative of the potential of flood and drought to occur, although they are not strict measures of the actual impact of flood and drought, since in some cases the climate based metrics do not correspond to observed reported events.

We can now turn our attention to the future projections. Figure 2 shows the additional number of ERSY due to global warming from 2011 to 2100 (i.e., the total number of ERSY at 2100 minus 90, where 90 is the ERSY number that would be obtained if there was no climate change) as projected by the model ensemble for the R99.9 and D25 metrics and the RCP8.5 and RCP2.6 scenarios. Note that both the R99.9 and D25 show positive additional stress due to climate change over the majority of land areas, which implies a prevailing projected increase in both the wet and dry extremes considered. Figure 2a shows that the increase in R99.9 adds more than 100 ERSY over most land areas in RCP8.5. Among the most sensitive regions (>250 additional ERSY) are parts of western North and South America, East and Central Africa, India, the Tibetan Plateau and South-east Asia. For the RCP2.6, the increase in stress due to R99.9 is much reduced, exceeding 100 ERSY only in small regions scattered across different continents.

For D25, the hotspots of increased stress (>100 additional ERSY) occur in areas of Central and South America, the Mediterranean basin and Central Europe, West and Central Africa, South-East Asia, and coastal Australia. Conversely, over the northern hemisphere high latitude regions, where mean precipitation is projected to increase,[12] the stress due to precipitation deficits actually decreases. Other areas where the stress due to D25 decreases are parts of eastern Africa, the Indian and Indochina peninsulas and northern China. Also for the D25, the areas of large changes of stress are much reduced in the RCP2.6, although still present in parts of South America, Africa, South-east Asia, and Australia. Figure 2 thus shows that the stress associated with both wet and
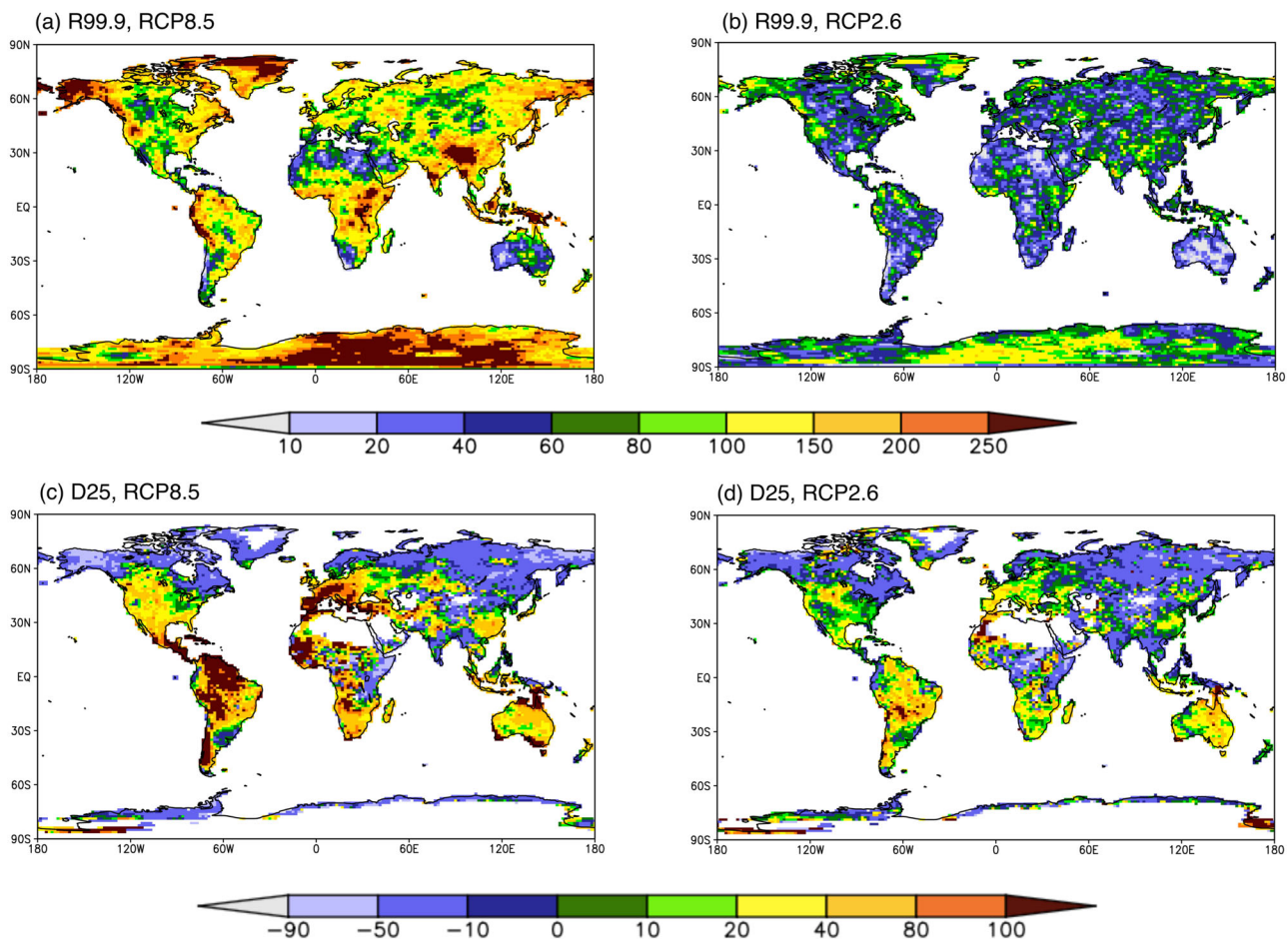

Fig. 2 **a** Ensemble average total cumulative additional stress index (CHS) due to changes in R99.9 for the period 2011–2100 in the RCP8.5 scenario. **b** Same as **a** but for RCP2.6; **c** Same as **a** but for changes in D25. **d** Same as **c** but for RCP2.6. Units are ERSY (see text) and the additional stress is calculated as the difference of the total value of ERSY for the period 2011–2100 minus 90 (number of ERSY without climate change)
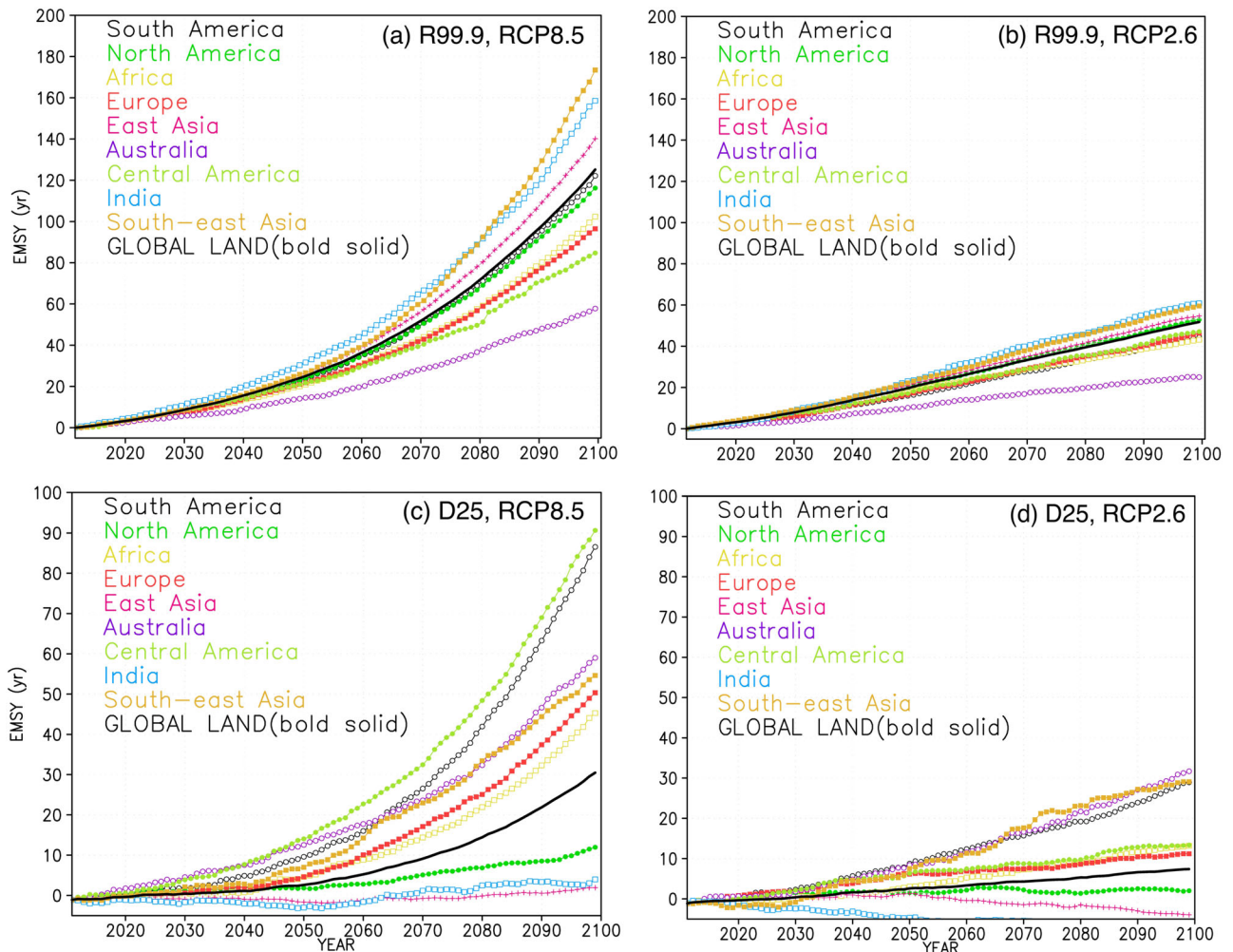
npj

Threatening levels of cumulative stress due to hydroclimatic
F Giorgi et al.

4

Fig. 3 Regionally averaged cumulative additional stress index (CHS) for the 9 selected regions of Figure S1 and global land throughout the period 2011–2100 due to **a** R99.9, RCP8.5; **b** R99.9, RCP2.6; **c** D25, RCP8.5; **d** D25, RCP2.6. Units are ERSY (see text) and the additional stress at a given year N is calculated as the total number of ERSY cumulated from 2011 to N minus the value (N—2011) (number of ERSY without climate change)

Table 1. Ensemble average number of additional ERSY by 2100 (AVE), ratio of ensemble average and inter-model standard deviation of additional ERSY by 2100 (AVE/Sigma), and number of models producing changes in additional ERSY by 2100 of the same sign as the ensemble average (N) for the different regions of Figure S1 and global land areas, the R99.9 and D25 metrics, and the RCP8.5 and RCP2.6 scenarios

REGION	R99.9, RCP8.5			R99.9, RCP2.6			D25, RCP8.5			D25, RCP2.6		
	AVE	AVE/Sigma	N	AVE	AVE/Sigma	N	AVE	AVE/Sigma	N	AVE	AVE/Sigma	N
South America	121.2	1.8	9	43.3	2.1	9	86.5	1.4	9	28.9	0.75	6
Europe	95.5	3.2	9	45.3	2.7	9	50.3	1.5	8	11.2	0.9	8
North America	115.2	3.7	9	51.9	2.1	9	12.0	0.5	6	2.0	0.1	4
East Asia	139.2	2.9	9	53.7	2.8	9	1.9	0.1	5	−4.0	−0.3	5
Africa	101.3	3.2	9	42.2	3.8	9	45.3	1.1	8	13.2	0.6	6
Australia	56.8	2.3	9	24.0	1.8	9	59.0	1.1	7	31.7	0.9	9
Central America	83.7	1.2	9	46.1	1.6	9	90.6	1.3	9	13.3	0.5	6
South-East Asia	172.4	1.3	8	58.5	1.7	8	54.6	0.6	6	29.1	0.4	5
India	157.6	3.3	9	59.8	1.7	9	4.0	0.1	4	−9.8	−1.0	7
Global Land	124.2	5.8	9	50.8	3.9	9	30.5	1.8	9	7.4	0.6	7

dry hydroclimatic extremes markedly increases due to climate change under the high-end RCP8.5 scenario, with pronounced spatial variability and a considerable avoided stress in the case of the RCP2.6.

Figure 3 shows the time evolution throughout the 21st century of the ensemble averaged projected CHS (additional ERSY) due to changes in R99.9 and D25 over the 9 regions of Figure S1, as well as over global land areas. On average, globally the R99.9 adds

Threatening levels of cumulative stress due to hydroclimatic
F Giorgi et al.

npj

5

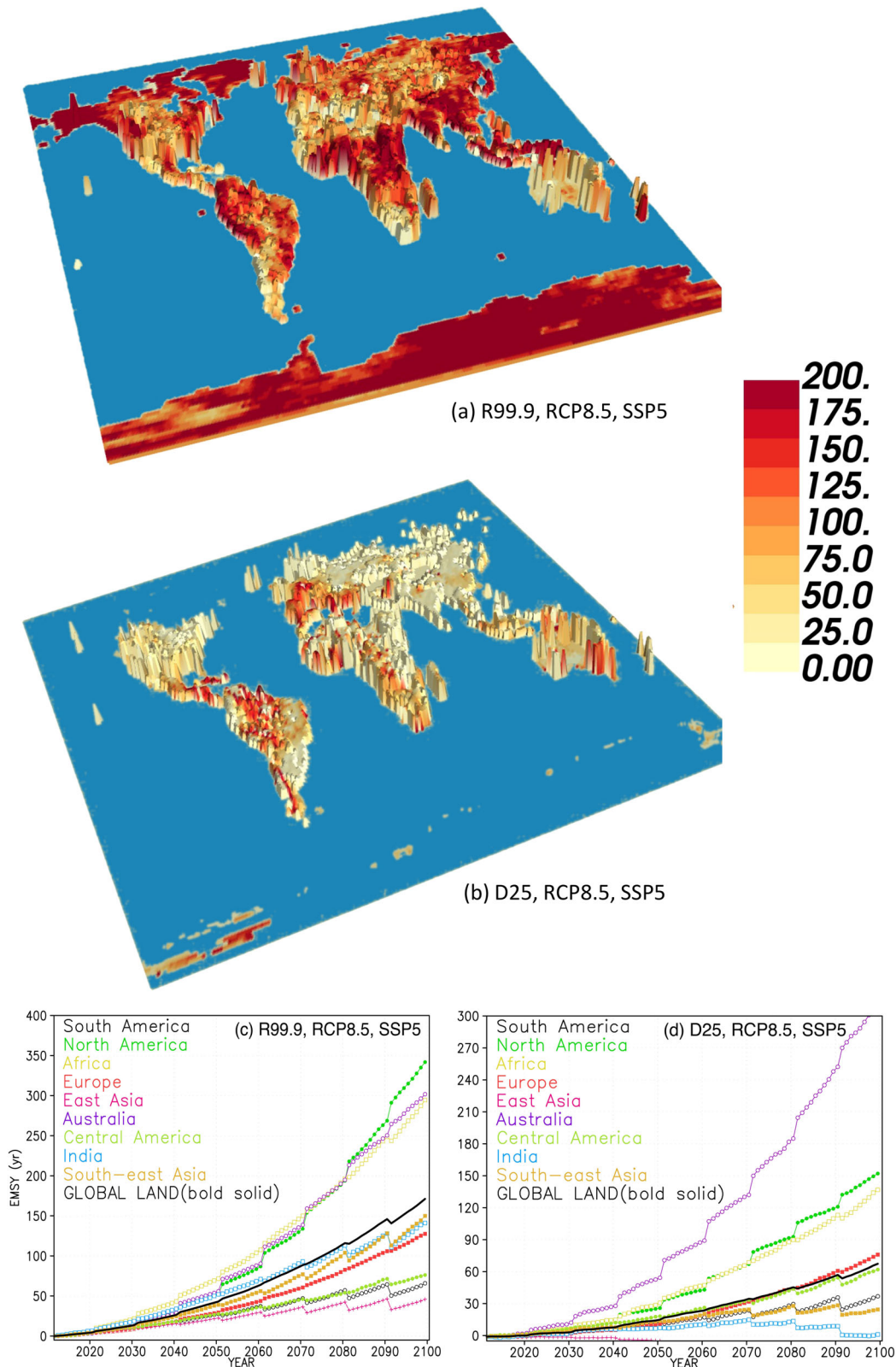(a) R99.9, RCP8.5, SSP5

(b) D25, RCP8.5, SSP5

Fig. 4   **a** Ensemble average total additional cumulative stress index (CHS) due to R99.9 for the period 2011–2100 (colors, units of ERSY, RCP8.5) overlaid to the ratio between population in 2100 and in 2010 at each grid box (SSP5). The units of the CHS are ERSY and the length of the vertical rods are proportional to the population ratio, with the longest rod being a ratio of 3. **b** Same as **a** but for the D25. **c** Regionally averaged population-weighted additional integrated cumulative stress index (ICHS) for the 9 selected regions of Figure S1 and global land throughout the period 2011–2100 due to R99.9 for the RCP8.5/SSP5 scenarios. **d** Same as **c** but for the D25. Units in **c** and **d** are ERSY (see text) and the additional stress at a given year N is calculated as the total number of ERSY cumulated from 2011 to N minus the value $(N—2011)$

Threatening levels of cumulative stress due to hydroclimatic
F Giorgi et al.

6

~125 ERSY by 2100 in RCP8.5. The regions with the strongest response are India, South-east and East Asia (~140–180 additional ERSY by 2100), where evidently the increase in extreme precipitation events is most pronounced. Conversely, Australia is the least responsive region in terms of R99.9 (~60 additional ERSY by 2100). In RCP2.6 the increase in R99.9 CHS is drastically reduced, ~50 ERSY by 2100 globally and ~60 ERSY in the most responsive regions. Concerning D25 (Fig. 3c, d), the regions with the largest increase of stress are Central and South America, up to 85–90 additional ERSY by 2100. India and East Asia experience little change in the regionally averaged D25 stress, which is however a compensation between areas of positive and negative changes (see Fig. 2). In RCP2.6 only South-east Asia, South America, and Australia show increases of D25 CHS (>25 ERSY by 2100), with decreases over India and East Asia.

Given the relatively small sample of GCMs utilized here, it is important to assess the robustness of the signals we find. Towards this goal, Table 1 shows for each region of Fig. 3, the number of models in which the simulated regionally averaged change signal by 2100 has the same sign as the ensemble average, along with the ratio of the ensemble-mean change signal by 2100 over the corresponding inter-model standard deviation. The latter can be considered as a measure of signal-to-noise ratio, and thus a value greater than 1 indicates more robustness in the result.

Table 1 shows that, for the R99-based index, in all regions (except south-east Asia for one model), all models agree on the sign of the change (increase) and the signal-to-noise ratio is always >1. Therefore, we conclude that the signal based on the

R99 metric is robust. More conflicting results are found for the D25 metric. For the RCP8.5 scenario, there is agreement across at least 6 out of 9 models on the sign of the signal (positive) over 7 out of 9 regions and globally, with the signal-to-noise ratio being greater than 1 over 5 regions and over global land. Therefore, although the projected change is less robust than for the R99.9 metric, we still find a prevalence of inter-model agreement. Conversely, for the RCP2.6 case the signal-to-noise ratio is mostly lower than 1, but this is associated to the fact that the change signal is generally small, and therefore this result could be interpreted by stating that for the low end RCP2.6 scenario there is little change in the D25 metric.

While Figs. 2 and 3 are only based on climate information, from the socio-economic point of view the potential stress also depends on the exposure of population, which is here included in the ICHS by weighting at each grid box the climate-derived variables by the corresponding time-varying population amounts (see Methods). Figure 4a and b overlay the R99.9 and D25 CHS by 2100 (additional ERSY, RCP8.5) to the population change in the SSP5 to illustrate how the two metrics interact. In the figure, the height of the vertical rod at each grid box is proportional to the ratio of population at year 2100 and that at year 2000, with the longest rod being a ratio of 3. The largest population increases occur over Australia, Africa, and North America. The latter two cases also show large increases in R99.9, while Australia and portions of Africa exhibit large increases in D25. Central America, Europe, and to a lesser extent South America also show relatively pronounced increases in both population and climate stress, while
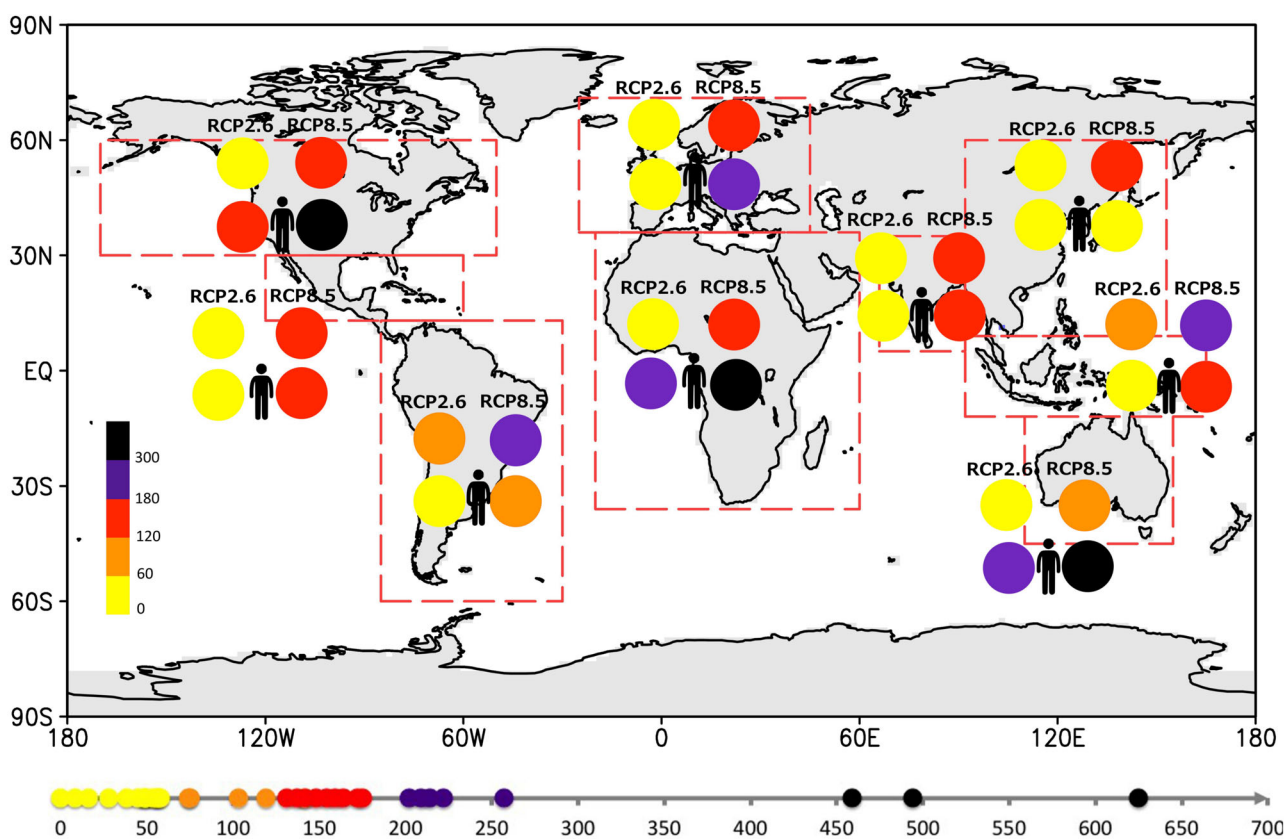

Fig. 5 Different total (R99.9 + D25) stress alarm thresholds (SAT) reached over each of the 9 regions of Figure S1 at year 2100. The SAT are: SAT1: 0–60 ERSY, yellow; SAT2: 60–120 ERSY, orange; SAT3: 120–180 ERSY, red; SAT4: 180–300 ERSY, purple; SAT5: >300 ERSY, black. For each region, the SAT is calculated for the CHS (climate only, top row) and the ICHS (including population weighting, bottom row), RCP2.5 (left column) and RCP8.5 (right column). The SAT thresholds are identified based on the clustering of the individual regional cases shown in the bottom bar, whose actual values are given in Table 1. The regional averages include only grid boxes with population in the reference period. The additional stress at year 2100 is calculated as the total number of ERSY cumulated from 2011 to 2100 minus 90 (number of ERSY without climate change)

Threatening levels of cumulative stress due to hydroclimatic
F Giorgi et al.

npj

7

the Asian regions exhibit large increases in R99.9 stress but small population growth (in fact for China even a reduction). This information combines to yield the regionally averaged ICHS stress (additional ERSY) for RCP8.5 presented in Fig. 4c and d (the corresponding information for RCP2.6 is provided in supplementary Figure S4).

Comparison of Fig. 4c and d with Fig. 2a and c, respectively, shows that the inclusion of population considerably modifies the picture of increased potential hydroclimatic stress. North America, Africa, and Australia emerge now as the primary stress hotspots, with increases in ICHS exceeding 270 ERSY for R99.9 and 120 ERSY for D25. Conversely, the East Asia region shows the smallest increases in R99.9-based potential stress and even a decrease in the D25-based one due to a projected decrease in population. Europe, Central and South America, India, and South-East Asia are characterized by the intermediate values of increased stress. A similar regional modulation of the potential hydroclimatic stress by population is found for the RCP2.6 scenario (Supplementary Figure S3), however with considerably smaller values in each region.

Our results are finally summarized in Fig. 5. Here we add together the additional ERSY due to R99.9 and D25 by the end of 2100 in order to measure the total additional potential stress due to extremes, although we recognize that in principle the risk associated with flood-prone and drought-prone events should be weighted differently. Also, in the calculation of the regional mean ERSY of Fig. 5, we only use populated grid boxes, assuming that the stress is only relevant in the presence of population. Results are presented for RCP8.5 and RCP2.6, both without (CHS) and with (ICHS) inclusion of population weighting. We define 5 "Stress Alarm Thresholds (SAT)" based on the additional ERSY by 2100, SAT1: 0–60, SAT2: 60–120, SAT3: 120–180, SAT4: 180–300, SAT5 > 300. These thresholds were identified from the clustering of the different cases shown on the bottom bar of Fig. 5, for which the actual values are reported in Table 2.

When only climate is considered (CHS), in RCP8.5 the SAT3 is reached in all regions except Australia, which is at the SAT2/SAT3 transition point, while South America and South-East Asia even reach the SAT4 level. In other words, on average all regions experience more than one equivalent century of additional potential stress due to increases in climate extremes. The population weighting (ICHS) produces a maximum SAT5 alarm level over North America, Africa, and Australia, with more than 400 ERSY of additional stress. Europe reaches the SAT4 level (203

additional ESRY), while all the other regions except South America and East Asia reach the SAT3 level. In RCP2.6, only North America, Africa, and Australia reach the SAT3 or SAT4 levels when population weighting is included, while East Asia shows even a decrease in stress (see Table 2) due to the reduction of population projected in that region.

DISCUSSION AND CONCLUSIONS

In this paper, we have analyzed the change in potential stress due to hydroclimatic extremes by introducing a new integrated cumulative stress index based on precipitation and population information. The flexibility of this index allows the implementation of more refined measures of socio-economic stress than used here. For example the actual cost estimated for the damage due to hydroclimatic extremes could be used as a metric of actual stress. In addition, the stress calculated for future periods could include metrics of adaptation policies or adaptive capacity. From the physical point of view, other types of extremes or climatic processes could be added, such as heat waves or storm surge events. Therefore, more accurate integrated measures of stress are certainly possible within our conceptual framework and the use of the ERSY as a metric of change in stress allows one to derive an easily understandable measure of added stress due to climate change.

An important assumption underlying our definition of the stress index is that the stress itself is linearly proportional to the excess or deficit precipitation amount. This is clearly a simplistic assumption, since the damage associated with an event could have a non-linear dependence on the event's intensity, and in fact not all R99.9 and D25 events might lead to significant damage. The availability of damage information for observed events could in principle enable the construction of better calibrated, and likely more realistic, stress-intensity functions. In addition, we do not include in our definition of cumulative stress the temporal succession of events, whereby events taking place for example on consecutive years could have a higher cumulative impact than events spaced by several years. This could however be easily implemented within our framework.

Notwithstanding these caveats, our calculations clearly indicate that for the high-end RCP8.5 scenario the increase of both wet and dry extremes can pose a significant risk for the sustainable development of societies throughout the 21st century in regions across all continents. This is particularly the case for North America, Africa, and Australia, where climate change, along with increased exposure based on population scenarios, produces a >400% increase in hydroclimatic stress. When population weighting is not included, South-east Asia and South America show the strongest responses, with over two equivalent centuries of hydroclimatic stress being added by climate change only.

Although more comprehensive calculations are needed to quantitatively refine our results, it is evident from our calculations that under the RCP2.6 scenario, which is close to the 2 °C stabilization target set in the Paris agreement,[21] the stress associated with increases of extreme events is considerably reduced throughout the globe, even if still substantial over some regions.

Table 2. Total number of additional stress years (units of EMSY, R99.9 + D25) for the period 2011–2100 over the different regions of Figure S1 for the cases without (CHS) and with (ICHS) population weighting and the RCP2.6 and RCP8.5 scenarios

REGIONS	CHS, RCP2.6	CHS, RCP8.5	ICHS, RCP2.6	ICHS, RCP8.5
South America	76	210	16	104
Nort America	58	132	155	495
Central America	59	176	39	138
Africa	49	160	258	460
Europe	57	149	29	203
East Asia	46	142	−48	8
Australia	56	120	216	627
India	53	165	48	142
South-east Asia	76	223	49	172

The averages include only grid boxes with population during the reference period 1981–2010

METHODS

The CHS is calculated as follows. For the case of extreme precipitation events, at each grid point of the common model grid, and for each model separately, we first calculate the value of the 99.9 percentile of daily precipitation events (R99.9) in the 30-year reference period 1981–2010, where a precipitation event is defined as having a daily precipitation amount greater than 1 mm/day. This procedure essentially identifies the threshold above which an event is expected to be "stressful" for a system, and the use of the 99.9 percentile implies the selection of the most

npj

Threatening levels of cumulative stress due to hydroclimatic
F Giorgi et al.

8

extreme events. We then calculate the cumulative precipitation in excess of the R99.9 threshold for all events identified in the 30-year reference period (1981–2010) and divide it by the number of years considered (in this case 30). This gives us the equivalent mean stress during one year due to extreme intensity events for the reference period, or $P_{R99.9\text{-ref}}$, defined as

$$P_{R99.9-ref} = \Sigma_{1981-2010} P_{R99.9}/30$$

where $P_{R99.9}$ is the precipitation in excess of the R99.9 threshold for daily events above the 99.9 percentile during each year of the reference period. The units of $P_{R99.9\text{-ref}}$ are thus mm/(day × yr) and the assumption here is that the stress is proportional to the amount of precipitation above the R99.9. To calculate the CHS due to R99.9 in the future period 2011–2100, $CHS_{R99.9}$, we accumulate the precipitation of daily events in excess of the 99.9 percentile threshold identified in the reference period, starting from 2011 until 2100 and normalize it by $P_{R99.9\text{-ref}}$. Therefore, for example, by the end of the century,

$$CHS_{R99.9-2100} = \Sigma_{2011-2100} P_{R99.9}/P_{R99.9-ref}$$

By way of this normalization, the units of $CHS_{R99.9}$ are years, and conceptually $CHS_{R99.9}$, which is calculated for each year of the twenty-first century, is a measure of the cumulative stress due to extreme events above the reference R99.9 threshold in units of Equivalent Reference Stress Years (ERSY). If we remove from the ERSY calculated at future year N (say 2050 or 2100) the number of years from the beginning of the accumulation period (i.e., 40 or 90 in the examples above) we remove the mean stress if climate was the same as in the reference period, and thus we obtain the additional number of ERSY due to climate change (or "additional ERSY"). For example, if for the period 2011–2100 we find 180 ERSY, we have 90 additional ERSY, meaning that climate change has doubled the amount of hydroclimatic stress with respect to the case in which climate would have been the same as during the reference period. In all the figures of the paper, we show the additional number of ERSY due to climate change.

To calculate the stress due to the precipitation deficit (D25) CHS_{D25}, we follow exactly the same procedure as for $CHS_{R99.9}$ with the difference that in place of $P_{R99.9}$ we use, for a given year, the precipitation deficit cumulated over sequences of at least 3 months in which the precipitation amount for that month (e.g., June) has a negative anomaly >25% of the mean climatology for the month (i.e., mean June precipitation) during the reference period 1981–2010. Thus, CHS_{D25} is also measured in ERSY but for stress due to precipitation deficits, where the assumption here is that the stress is proportional to the amount of the precipitation deficit itself.

A few caveats need to be taken into account concerning these definitions. First, because of the use of precipitation deficits in mm/day for the calculation of CHS_{D25}, this index is dominated by deficits during the rainy season. Second, while the use of R99.9 makes the $CHS_{R99.9}$ index always computable, it is possible that at a grid box no month during the reference period has a negative anomaly greater then 25%, particularly in models with low interannual variability. These cases, which would lead to a division by 0 in the calculation of CHS_{D25}, are discarded from the analysis. This procedure also effectively removes desert areas from the calculation.

The CHS is computed only based on precipitation information, however socio-economic information such as population exposure or damage cost, could be included to refine the definition of stress, leading to the Integrated Cumulative Hydroclimatic Stress index (or ICHS). Here we calculate the ICHS by incorporating population as a metric of exposure. Specifically, we follow exactly the same procedure as for the CHS, but at each grid box the precipitation extreme or deficit values are multiplied by the population estimate at that grid box which, for the reference period and the RCP8.5 and RCP2.6 scenarios are taken from the IIASA Shared Socioeconomic Pathways (SSPs) and related Integrated Assessment scenarios.[14] The SSPs are part of a new framework that the climate change research community has adopted to facilitate the integrated analysis of future climate impacts, vulnerabilities, adaptation, and mitigation. Specifically, the SSP1 and SSP5 are used here as population scenarios for RCP2.6 and RCP8.5,[14] respectively. The population data are updated every 10 years, which yields the "steps" shown by the curves of Fig. 4 and S2. By this definition, grid boxes with no population in the reference period are automatically removed from the calculations of the ICHS.

Finally, the ensemble of CMIP5 models used in the analysis is reported in supplementary Table S1.[22–29]

AUTHOR CONTRIBUTIONS
F.G. conceived the study, contributed to the analysis, and wrote the paper. E.C. and F. R. contributed to the analysis and the production of figures and the text.

ADDITIONAL INFORMATION
Supplementary information accompanies the paper on the *npj Climate and Atmospheric Science* website (https://doi.org/10.1038/s41612-018-0028-6).

Competing interests: The authors declare no competing interests.

Publisher's note Springer Nature remains neutral with regard to jurisdictional claims in published maps and institutional affiliations.

REFERENCES
1. Intergovernmental Panel on Climate Change (IPCC) in *IPCC Special Report* (eds Field, C. B. et al.) 582 (Cambridge University Press, Cambridge, UK, 2012).
2. Easterling, D. R., Meehl, G. A., Parmesan, C., Changnon, S. A. & Mearns, L. O. Climate extremes: observations, modeling and impacts. *Science* **289**, 2068–2074 (2000).
3. Trenberth, K. E., Dai, A., Rasmussen, R. & Parsons, D. The changing character of precipitation. *Bull. Am. Meteorol. Soc.* **84**, 1205–1217 (2003).
4. Held, I. M. & Soden, B. J. Robust responses of the hydrological cycle to global warming. *J. Clim.* **19**, 5686–5699 (2006).
5. Tebaldi, C., Hayhoe, K., Arblaster, J. M. & Meehl, G. A. Going to the extremes: an intercomparison of model-simulated historical and future changes in extreme events. *Clim. Change* **79**, 185–211 (2006).
6. Christensen, J. H. & Christensen, O. B. Climate modeling: severe summertime flooding in Europe. *Nature* **421**, 805–806 (2003).
7. Allan, R. P. & Soden, B. J. Atmospheric warming and the amplification of precipitation extremes. *Science* **321**, 1481–1484 (2008).
8. Giorgi, F. et al. Higher hydroclimatic intensity with global warming. *J. Clim.* **24**, 5309–5324 (2011).
9. Sillmann, J., Kharin, V. V., Zwiers, F. V., Zhang, X. & Bronaugh, D. Climate extreme indices in the CMIP5 multimodel ensemble: Part 2. Future climate projections. *J. Geophys. Res.* **118**, 2473–2493 (2013).
10. Giorgi, F. et al. Changes in extremes and hydroclimatic regimes in the CREMA ensemble projections. *Clim. Change* **125**, 39–51 (2014).
11. Giorgi F., Coppola E. & Raffaele F. A consistent picture of the hydroclimatic response to global warming from multiple indices: modeling and observations. *J. Geophys. Res.* **119**, 11695–11708 (2014).
12. Taylor, K. E., Stouffer, R. J. & Meehl, G. A. An overview of CMIP5 and the experiment design. *Bull. Am. Meteor. Soc.* **93**, 485–498 (2012).
13. Moss, R. H. et al. The next generation of scenarios for climate change research and assessment. *Nature* **463**, 747–756 (2010).
14. Rihai, K. et al. The shared socioeconomic pathways and their energy, land use, and greenhouse gas emissions implications: an overview. *Global Environ. Chang.* **42**, 148–152 (2016).
15. Jones, C. D. et al. The HadGEM2-ES implementation of CMIP5 centennial simulations. *Geosci. Model Dev.* **4**, 543–570 (2011).
16. Chen, M. et al. Assessing objective techniques for gauge-based analyses of global daily precipitation. *J. Geophys. Res.* **113**, D04110 (2008).
17. Kharin, V. V., Zwiers, F. W. & Zhang, X. Intercomparison of near surface temperature and precipitation extremes in AMIP-2 simulations, reanalyses and observations. *J. Clim.* **18**, 5201–5233 (2005).
18. Chen, C. T. & Knutson, T. On the verification and comparison of extreme rainfall indices from climate models. *J. Clim.* **21**, 1605–1621 (2008).
19. Sillmann, J., Kharin, V. V., Zhang, X., Zwiers, F. W. & Bronaugh, D. Climate xtreme indices in the CMIP5 multimodel ensemble. Part I: Model evaluation in the present climate. *J. Geophys. Res.* **118**, 1716–1733 (2013).

Threatening levels of cumulative stress due to hydroclimatic
F Giorgi et al.

npj

9

20. Wehner, M. F., Smith, R. L., Bala, G. & Duffy, P. The effect of horizontal resolution on simulaiton of very extreme US precipitaiton events in a global atmosphere model. *Clim. Dyn.* **24**, 241–247 (2010).
21. IPCC. in *Climate Change 2013. The Physical Science Basis. Contribution of Working Group I to the Fifth Assessment Report of the Intergovernmental Panel on Climate Change* (eds Stocker, T. F. et al.) 29 (Cambridge University Press, Cambridge, UK, 2013).
22. Jungclaus, J. H. et al. Characteristics of the ocean simulations in the Max Planck InstituteOcean Model (MPIOM) the ocean component of the MPI-Earth system model. *J. Adv. Model. Earth Syst.* **5**, 422–446 (2013).
23. Delworth, T. L. et al. GFDL's CM2 global coupled climate models. Part I: formulation and simulation characteristics. *J. Clim.* **19**, 643–674 (2006).
24. Gent, P. R. et al. The community climate system model version 4. *J. Clim.* **24**, 4973–4991 (2011).
25. Dufresne, J.L. et al. Climate change projections using the IPSL-CM5 earth system model: from CMIP3 to CMIP5. *Clim. Dyn.* **40**, 2123–2165 (2013).
26. Watanabe, S. et al. MIROC-ESM 2010: model description and basic results of CMIP5-20c3m experiments. *Geosci. Model Dev.* **4**, 845–872 (2011).
27. Collier M. A., et al. The CSIRO-Mk3.6.0Atmosphere-Ocean GCM: participation in CMIP5 and data publication. In *19th International Congress on Modelling and Simulation, Perth, Australia* 12–16. https://www.mssanz.org.au/modsim2011 (2011).
28. Voldoire, A. et al. The CNRM-CM5.1 global climate model: description and basic evaluation. *Clim. Dyn.* **40**, 2091–2121 (2011).
29. Chylek, P. et al. Observed and model simulated 20th century Arctic temperature variability: Canadian Earth System Model CanESM2. *Atmos. Chem. Phys.* **11**, 22893–22907 (2011).